

**DIMMING DC-DC LED DRIVERS:
POWER LOSSES, LUMINOUS EFFICIENCY & BEST-IN-CLASS**

A Dissertation
Presented to
The Academic Faculty

by

Vasu Gupta

In Partial Fulfillment
of the Requirements for the Degree
Master of Science in the
Electrical and Computer Engineering

Georgia Institute of Technology
December 2021

COPYRIGHT © 2021 BY VASU GUPTA

**DIMMING DC-DC LED DRIVERS:
POWER LOSSES, LUMINOUS EFFICIENCY & BEST-IN-CLASS**

Approved by:

Dr. Gabriel A. Rincón-Mora, Advisor
School of Electrical and Computer Engineering
Georgia Institute of Technology

Dr. Deepakraj M. Divan
School of Electrical and Computer Engineering
Georgia Institute of Technology

Dr. Maryam Saeedifard
School of Electrical and Computer Engineering
Georgia Institute of Technology

Date Approved: December 10, 2021

ACKNOWLEDGEMENTS

I would like to express my deepest appreciation to my advisor, Prof. Gabriel A. Rincón-Mora, for his research advise, imparting priceless life lessons and guiding me through my M.S. degree. I have learnt a lot from his technical insights in analog and power ICs, attention to details, and professionalism. I will make use of these for the rest of my career.

The financial and logistical support of Analog Devices Inc. (ADI) has been instrumental to my graduate study, and I honestly appreciate it. Moreover, I would like to thank my mentor, Dr. Dongwon Kwon, for his invaluable support during my internship at ADI and M.S. degree.

I want to specially thank my colleagues Tianyu, Avinash, Guillaume, Pengyu and Qian at the Georgia Tech Analog, Power and Energy Lab (GTAPE) for day-to-day discussions and technical feedback. I also wish to acknowledge the administrative assistance of Ms. Tasha Torrence and Mr. Andrew Stargill from Georgia Tech's ECE graduate office all through the program.

I would like to extend special thanks and gratitude to my parents, family members and my friends Anubhav, Girish, and Mohit. I wish to thank Awani for her patience, encouragement, and love throughout my degree and while finishing this thesis. Without their unwavering support, none of my accomplishments would have been possible.

Finally, I thank Prof. Deepakraj M. Divan and Prof. Maryam Saaedifard for their insightful feedback and for being a part of my thesis advisory committee.

TABLE OF CONTENTS

ACKNOWLEDGEMENTS	iii
LIST OF TABLES	v
LIST OF FIGURES	vi
SUMMARY	viii
CHAPTER 1. LIGHT-EMITTING DIODES	1
1.1 Applications	1
1.2 Electrical and Optical Characteristics	2
1.3 Dimming	4
1.4 Challenges and State of the Art in dimming	5
1.5 Research Objective	7
1.6 Summary	7
CHAPTER 2. DC-SOURCED LED DRIVERS	8
2.1 Load Configurations	8
2.2 DC–DC LED Driver Topologies	9
2.2.1 Linear	10
2.2.2 Buck–Boost SL	11
2.2.3 Buck SL	12
2.2.4 Boost SL	13
2.3 Summary & Conclusions	14
CHAPTER 3. ANALOG DIMMING	15
3.1 Dimming Range	17
3.2 Luminous Efficiency	17
3.3 Summary	20
CHAPTER 4. DUTY-CYCLED DIMMING	21
4.1 Shutdown	21
4.2 Shunt-Switched	24
4.3 Series-Switched	28
4.4 Luminous Efficiency	30
4.5 Summary	30
CHAPTER 5. CONCLUSIONS AND FUTURE WORK	31
5.1 Conclusions	31
5.2 Future Directions	33
REFERENCES	34

LIST OF TABLES

	Page
Table 5-1. Comparison of analog and duty-cycled dimming.	32

LIST OF FIGURES

	Page
Figure 1-1. LEDs in backlit TV, edge-lit mobile display, and automotive headlight.	1
Figure 1-2. A typical automotive electrical system [12].	2
Figure 1-3. Luminous flux vs. output current for automotive LEDs at constant T_J .	3
Figure 1-4. Normalized luminous flux vs. output current for automotive LEDs.	3
Figure 1-5. Luminous flux vs. output current for four CREE XP-E2 LEDs.	4
Figure 1-6. Output voltage and current vs. luminous flux.	4
Figure 1-7. Luminous efficiency vs. LED current in state of the art [26].	6
Figure 2-1. LED driver system.	8
Figure 2-2. (a) Forward, (b) Reverse and Inverting LED load configurations.	9
Figure 2-3. Multi-channel driver with a linear current source and switching pre-regulator [23].	10
Figure 2-4. NMOS based linear LED driver.	10
Figure 2-5. Forward buck–boost SL driver.	11
Figure 2-6. Inverting buck–boost SL driver.	12
Figure 2-7. Buck SL driver.	12
Figure 2-8. Boost SL driver.	13
Figure 3-1. Switched inductor buck–boost LED driver power stage.	15
Figure 3-2. Simulated CCM operation.	16
Figure 3-3. Simulated DCM operation.	16
Figure 3-4. Luminous flux vs. output current for four CREE XP-E2 LEDs.	18
Figure 3-5. Output voltage and current vs. luminous flux.	18
Figure 3-6. Simulated conversion efficiency vs. output current.	19

Figure 3-7. Modeled and simulated input power vs. luminous flux	19
Figure 3-8. Modeled and simulated luminous efficiency vs. luminous flux.	20
Figure 4-1. Shutdown duty-cycled dimming operation.	21
Figure 4-2. $t_{R/F}$ approximations for shutdown.	23
Figure 4-3. Input power and P_{PWM} vs. luminous flux.	24
Figure 4-4. Breakdown of power losses in analog and PWM dimming.	24
Figure 4-5. SL LED driver for shunt-switched dimming.	25
Figure 4-6. Shunt-switched PWM operation.	25
Figure 4-7. Breakdown of power losses in shunt-switched PWM dimming.	26
Figure 4-8. $t_{R/F}$ for shunt-switched PWM.	27
Figure 4-9. SL LED driver for series-switched dimming.	28
Figure 4-10. Series-switched PWM operation.	28
Figure 4-11. Breakdown of power losses in series-switched PWM dimming.	29
Figure 4-12. $t_{R/F}$ for series-switched PWM.	30
Figure 5-1. Buck and boost implementations of series- and shunt-switched PWM.	32

SUMMARY

Light-Emitting Diodes (LED) have become pervasive in modern lighting systems. With advantages such as fast response time, compact size, high reliability, and high luminous efficiency, they are used in automotive, general lighting, and industrial applications. These current-controlled solid-state devices require AC- and DC-sourced power electronic systems to regulate their brightness.

Thermal constraints in these high-power compact systems demand high luminous efficiency. Luminous efficiency η_L is light delivered per unit input power P_{IN} . It is a cascaded measure of power-conversion efficiency η_C , a fraction of P_{IN} delivered to the load and LED's electro-optical efficiency. The latter is manufacturer-defined, whereas the former is a key design parameter.

Linear regulators, even with low dropouts (LDO), fail to meet η_C expectations owing to high ohmic power losses at typical greater than 100 mA loads. Switched inductor (SL) converters, however, can output a larger fraction of power they draw from the input, often greater than 85% for moderate to high P_{IN} . The fundamental reason for this is low ohmic losses, and that is because switches in the network only drop a few millivolts. Moreover, SLs can boost the input v_{IN} to a higher output voltage, which LDOs cannot. Therefore, SLs can power low- v_{IN} LED driver applications.

LED drivers regulate the LED's average current that sets their luminous output, where dimming is an important attribute. Dimming techniques fall in one of two categories: "analog" or "duty-cycled" (pulse-width-modulated), and duty-cycled (PWM) dimming decompose into two further classes: series- or shunt-switched, each with its unique design challenges,

advantages, and limitations. However, a comprehensive analysis of dimming techniques, corresponding power losses, and their dimming capabilities for DC–DC applications is lacking in the literature.

This research analyzes, models, and compares dimming techniques for SL LED drivers. The luminous output of high-power LEDs is a nonlinear function of the forward current, exhibiting a concave behavior such that the slope of the luminous output decreases and saturates at higher current levels. As a result, LED’s brightness is not only uniquely determined by the average LED current but also by the way it is driven. This behavior complicates LED dimming.

A buck–boost power stage is designed and simulated for a 12 V DC-input automotive application delivering up to 1 A of current to four power LEDs. Followed by theoretical analysis and modeling, this research quantifies and compares the techniques on multiple parameters such as power losses, luminous efficiency, and dimming range. The results are validated using SPICE simulations.

This research reveals and verifies that analog dimming yields the highest luminous efficiency, up to 57% more. This is because duty-cycled dimming suffers from a fundamental PWM-power loss, a byproduct of LED’s luminous non-linearity. Moreover, discontinuous conduction in analog furnishes the widest dimming range. Overall, analog dimming outperforms PWM in power losses, majority of η_L , and achieves 0-100% dimming range, emerging as the best-in-class.

CHAPTER 1. LIGHT-EMITTING DIODES

1.1 Applications

Ever since the discovery of electroluminescence more than a century ago [1], breakthroughs in high-power solid-state devices have pushed light-emitting diodes (LEDs) to the forefront in modern lighting systems [2]. LEDs, owing to their compact size, high reliability [3], fast response time, and more importantly high electro-optical conversion efficiency [4]–[5] have largely substituted conventional incandescent and chloro-florescent lights in high-power (> 1 W) applications [6]–[7]. These include AC-sourced lighting, televisions, mobile devices, and battery-operated automotive, among many others as shown in Fig. 1-1 [7]–[11].



Figure 1-1. LEDs in backlit TV, edge-lit mobile display, and automotive headlight [3].

Automotive applications are of particular interest because of the need for multiple light sources in a vehicle, for example, headlight modules, interior, tail, and brake lights. Furthermore, automotive lighting can require designs that serve a function and form for styling, personalization, and safety [7], and consequently, adding to the total power and quantity of electronic components driving these LED-based use cases. This leads to a push for higher power and eventually necessitates better thermal management in the electronics powering them.

Modern automotive systems are typically powered by a 12 V lead-acid battery which depending on irregular conditions such as cold crank, alternator load dump or jump-start can develop transients between 3 V to 35 V [12]–[13] as shown in Fig. 1-2. In traditional fuel-powered vehicles, the engine drives a three-phase generator (also called as alternator) whose rectified output is delivered to the 12 V battery. Unwanted voltage spikes and transients are harmful and thus necessitate the use of intermediate DC–DC regulators represented as load in Fig. 1-2. The ones that regulate LED current are called LED drivers [4].

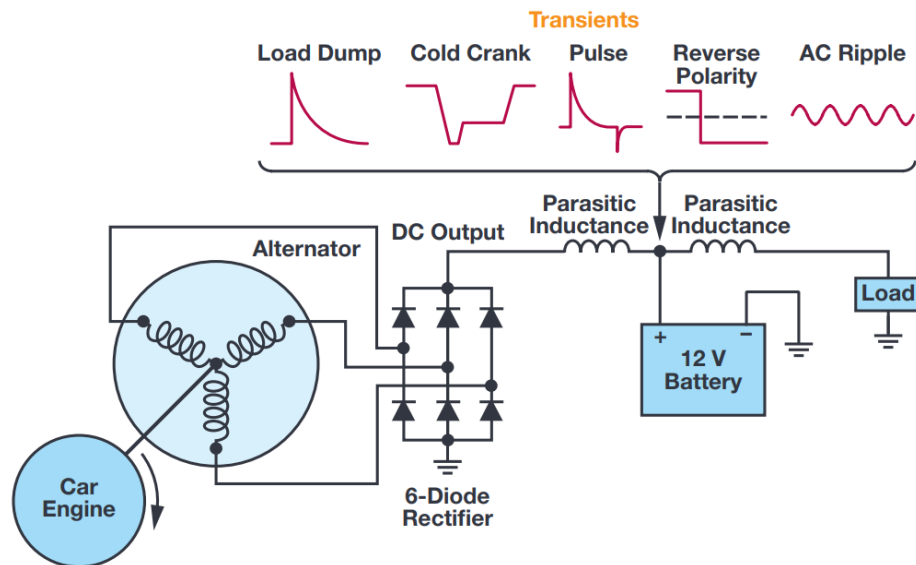


Figure 1-2. A typical automotive electrical system [12].

1.2 Electrical and Optical Characteristics

Electrically, LEDs behave like a p-n junction diode and exhibit exponential I-V characteristics. LED brightness is inherently non-linear with its driving current [9], that is, it varies linearly for small currents and tends to saturate at higher current levels. This phenomenon is also reflected in a majority of the automotive LEDs manufactured by various vendors as illustrated [14]–[21] in Fig. 1-3. Although these products span over a wide range of luminous output and

LED current, a normalization over these parameters shows a similar luminosity saturation phenomenon as depicted in Fig. 1-4.

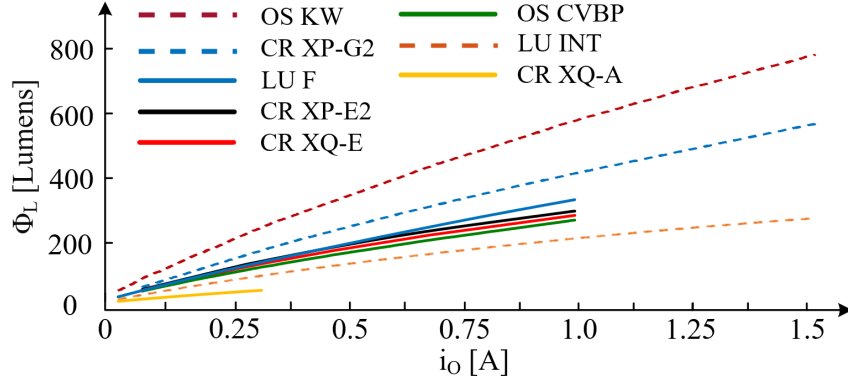


Figure 1-3. Luminous flux vs. output current for automotive LEDs at constant T_j .

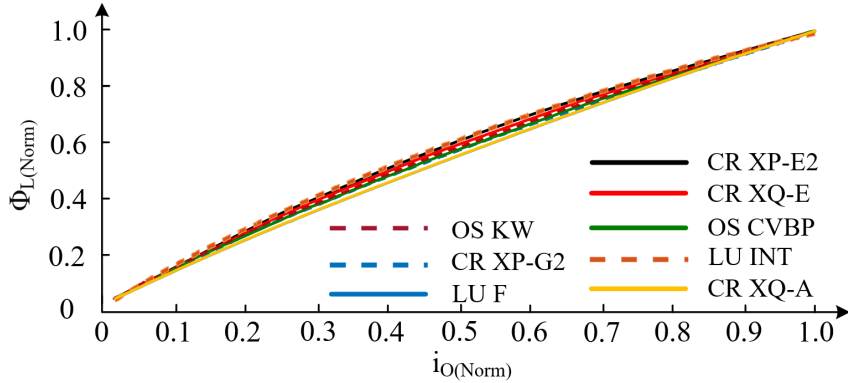


Figure 1-4. Normalized luminous flux vs. output current for automotive LEDs.

As Fig. 1.4 shows, ϕ_L (extracted from datasheet) varies exponentially with LED current i_O :

$$\phi_L \approx N_D \phi_k \left(1 - e^{-i_O/I_k}\right), \quad (1.1)$$

where N_D is the number of series-connected LEDs (*i.e.*, 4), and $\phi_k = 356$ and $I_k = 1.07$ are the modeled LED-dependent constants for cool-white CREE XP-E2 LED [17]. (1.1) can be rewritten as a logarithmic function of ϕ_L as:

$$i_o = \frac{1}{I_k} \ln \left(1 - \frac{\phi_L}{N_D \phi_k} \right)^{-1}. \quad (1.2)$$

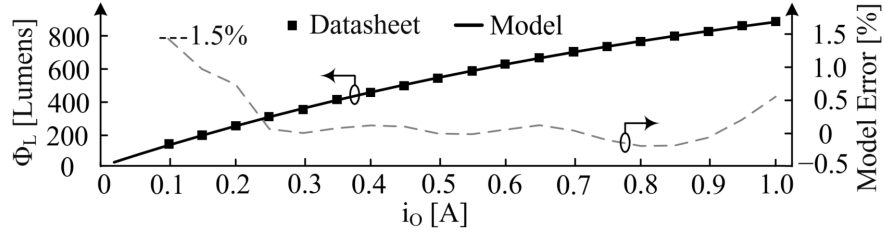


Figure 1-5. Luminous flux vs. output current for four CREE XP-E2 LEDs.

Since LEDs are electrically modeled as diodes [22], output voltage v_o as shown in Fig. 1-6 is a logarithmic and linear R_D translation of i_o :

$$v_o = N_D (v_D + v_R) = N_D \left(n_I v_T \ln \frac{i_o}{I_S} + i_o R_D \right), \quad (1.3)$$

where v_D is diode voltage, v_R is the voltage across LED parasitic resistance R_D , n_I is the diode non-ideality factor and I_S is the reverse saturation current.

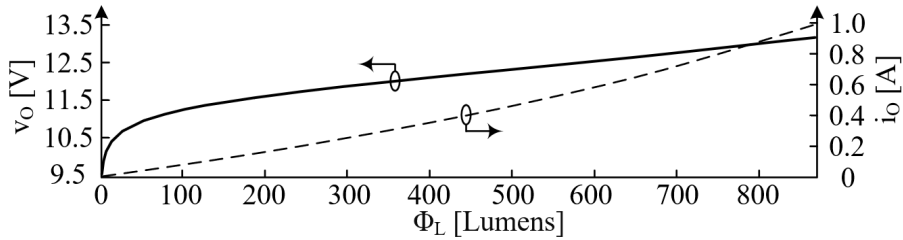


Figure 1-6. Output voltage and current vs. luminous flux.

1.3 Dimming

LED drivers regulate DC-output current i_o instead of voltage because LED's brightness is proportional to i_o [22]–[23]. Controlling i_o to vary the brightness is referred to as dimming, a vital feature of LED drivers. LEDs are more robust than their incandescent and fluorescent

counterparts and enable a flicker-free and smooth dimming operation [3]. Flickering is defined as a rapid and repeated change in brightness over time, which is minimal at dimming frequencies of over 100 Hz.

Dimming techniques are classified into two categories, analog and duty-cycled (or PWM) [1]. In analog, i_o is varied continuously whereas in duty-cycled, it is pulse-width modulated to an average during a fixed period. For automotive, this frequency falls in a range of 0.1-1 kHz [8]. Duty-cycled (PWM) dimming decomposes into two further classes: series- or shunt-switched. These techniques are further analyzed in Chapters 3 and 4. Dimming range captures the dimming capability of a driver, which electrically translates to the least average i_o possible.

1.4 Challenges and State of the Art in dimming

Dimming techniques for LED driver systems discussed further in Chapter 2, have been studied extensively by both industry [13], [24]–[25] and academia [1], [26]. The efficiency of a light source is measured in lumens-per-watt, which indicates the amount of light emitted per consumed unit power. State-of-the-art covering LED dimming falls into two general categories, first, the ones that provide a qualitative overview of relevant techniques. These reviews cater to a more general audience and do not delve into system implementations and related trade-offs. The ones that do fall under the second category [1], [26], however, do not accommodate LED driver artifacts such as η_c or are lacking in their coverage of all techniques. Whereas some of these provide an abstract understanding, all are limited in their analysis and fail to provide a coherent evaluation in the context of a complete power electronic system.

In [1], [26], authors analyze, evaluate, and compare analog and PWM dimming techniques based on isolated LED luminous output characteristic variations with different

forward current waveforms. The analysis proves as a good starting point but falls short of delving into a complete system, that is, system non-idealities such as conversion efficiency, limited dimming range, and additional power losses have been ignored. Fig. 1-7 depicts the achieved luminous efficiency in analog and PWM dimming with an isolated LED. As seen and would be highlighted in Chapter 3, the luminous efficiency increases with lower currents. Unfortunately, this changes when LED driver conversion efficiency is considered. As seen later in Chapter 3, these losses would dominate at lower currents.

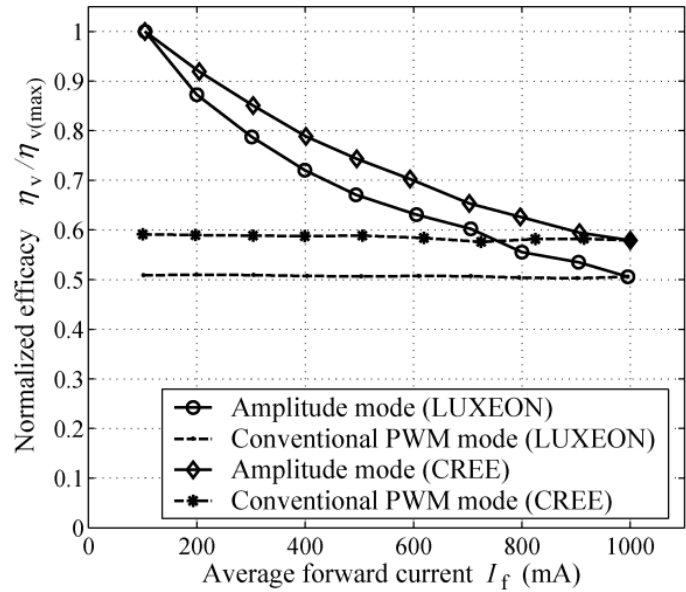


Figure 1-7. Luminous efficiency vs. LED current in state of the art [26].

On the other hand, research such as [13], [24]–[25] detail variations in dimming techniques and their pros and cons but fail to quantify the differences. That is, the analysis is not rigorous, and the comparisons are anecdotal. Moreover, these as well forego driver circuitry and its effects on the dimming parameters.

1.5 Research Objective

The proposed research aims to cover key attributes in the analog and duty-cycled (PWM) dimming techniques in switched inductor DC–DC LED drivers. The objective of the research is three-fold, first, to design a representative LED driver system for a peak 1 A output current automotive application. Second, to simulate the state-of-the-art dimming techniques and accurately model their attributes and, third, to evaluate their advantages, disadvantages and reveal the best-in-class technique. This research also aims to systematically quantify lesser understood effects of power stage losses on luminous efficiency in duty-cycled dimming techniques and explain the dependence of dimming range on output capacitance, LED current, and output voltages.

1.6 Summary

This chapter presents an overview of light-emitting diodes, their applications, and luminous and electrical characteristics. It briefly explains dimming and highlights key dimming techniques and the limitations of the state-of-the-art in assessing those. Followed by briefing their use in modern applications, a summary of automotive LED applications, their requirements, and challenges is presented. A survey of state-of-the-art automotive LEDs reveals their luminous efficiency to be a non-linear saturating function of its forward current, which is modeled and matched with its datasheet using exponential-like expressions. In the following chapter, state-of-the-art in LED driver systems are presented with an operational understanding of popular switched-inductor DC–DC LED driver topologies.

CHAPTER 2. DC-SOURCED LED DRIVERS

LED's luminous output is proportional to LED current. Since LEDs are essentially diodes, a slight variation in applied voltage can lead to large fluctuation in its current and therefore, brightness. Furthermore, as the temperature rises, a negative temperature coefficient of forward voltage exacerbates this effect thus complicating voltage regulation. As such, current regulation is preferable. Since LEDs operate on DC currents, AC-powered LED driver systems constitute an intermediate AC–DC conversion step followed by a DC–DC regulation stage [9], which depending on the topology can deliver power to reverse, inverting, and non-inverting load configurations [8] as Fig. 2-1 depicts.

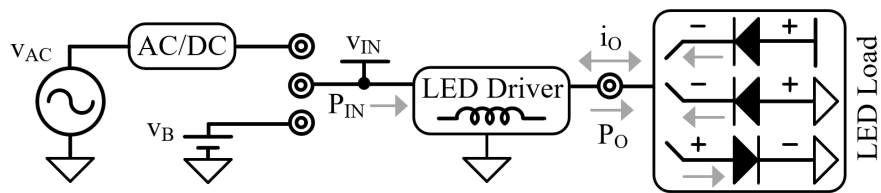


Figure 2-1. LED driver system.

The DC–DC current regulation stage can vary depending on the application, which usually dictates input and output voltages, total delivered power, system efficiency, and space constraints. This chapter highlights all state-of-the-art switched-inductor variations of DC-sourced LED topologies.

2.1 Load Configurations

The typical LED driver system can power multiple LED arrangements as illustrated in Figs. 2-1 and 2-2. These configurations are a consequence of the preceding DC–DC power stage

design, that can output positive or negative voltages for forward, reverse, or inverting topologies discussed in the next section.

LED load is configured as ‘forward’ (as shown in Fig. 2-2 (a)) when the total power delivered, a multiple of the current i_{LED} and voltage v_O , is positive and the LED current flows from v_O , which is connected to the cathode and powers the LEDs to a ground-connected anode. Since popular DC–DC convertor topologies like buck, boost, buck–boost are typically configured as forward [8], [22]–[24], it is the most common one.

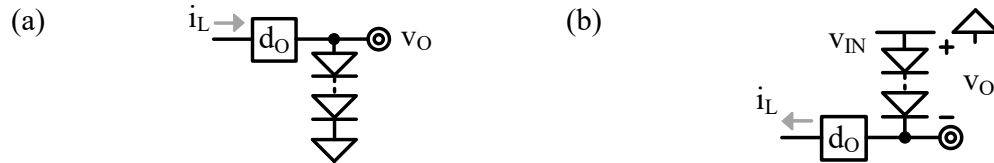


Figure 2-2. (a) Forward, (b) reverse and inverting LED load configurations.

In ‘reverse’, unlike forward, the LEDs are directly powered via input v_{IN} as Fig. 2.2 (b) illustrates. This is mostly used in buck LED drivers where a ground-connected NMOS allows a simpler and less noisy inductor current sensing for feedback control [30]. However, since LEDs drop positive voltage when forward-biased, SLs in reverse cannot boost. In inverting, the cathode is grounded, and the power stage regulates a negative voltage for the corresponding LED current. The anode is connected to the power stage output which on average is positive but lower than v_{IN} in reverse and negative in inverting configuration.

2.2 DC–DC LED Driver Topologies

The DC–DC stage as depicted in Fig. 2.1 can be implemented using various topologies that can be broadly categorized as linear and switched inductor [26]. This section goes over each of those, their basic operation, use cases, and advantages and disadvantages.

2.2.1 Linear

Linear regulators are one of the simplest circuit topologies used in LED driver applications. Depending on the input voltage, they can source from either a pre-regulating switching regulator [23] as shown in Fig. 2-3 or directly from the input.

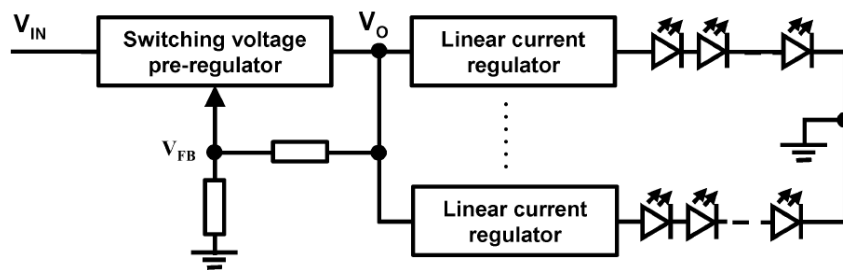


Figure 2-3. Multi-channel driver with a linear current source and switching pre-regulator [23].

Figure 2.4 illustrates a linear LED driver topology. In this case, the LEDs are connected in reverse load configuration. Error amplifier A_V regulates the resistor voltage v_{FB} and hence LED current i_{LED} (v_{FB}/i_{LED}) by the virtue of negative feedback across the pass transistor N_P .

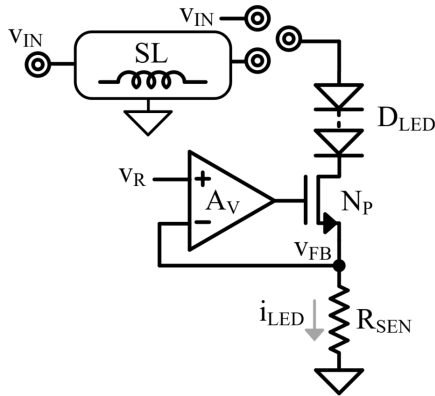


Figure 2-4. NMOS based linear LED driver.

Since i_{LED} drops voltage across R_{SEN} and switch N_P , there's an additional ohmic power loss associated with linear regulators. This effectively puts their usage outside the high-current applications where conversion efficiency is important. However, contrary to switched inductors, since these do not require additional magnetic and charge storage elements such as inductors or capacitors (no i_O load dumps), they are cheap to manufacture and consume little board space. Often linear regulators are seen in space-constrained, low power applications such as mobile device displays and indicator LEDs [6], [9].

2.2.2 Buck–Boost SL

As the name implies, buck–boost switched inductor *bucks* or *boosts* v_{IN} to a lower or higher v_O as illustrated in Fig. 2-5 [27]. In the case of LED drivers, this positive output voltage v_O is dropped across the series-connected diodes. Switches S_{EI} and S_{EG} energize the inductor L_X by drawing input power from v_{IN} . Subsequently, drain switches S_{DG} and S_{DO} de-energize L_X to v_O . Buck–boost topologies can be configured in asynchronous and synchronous modes, that is, drain switches S_{DG} and S_{DO} can be replaced by P-N junction diodes or MOSFET-based switches.

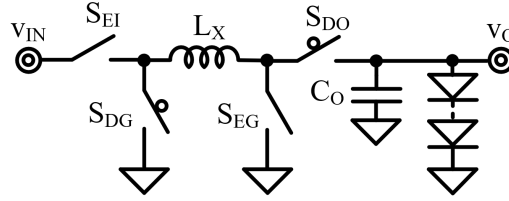


Figure 2-5. Forward buck–boost SL driver.

Buck–boost LED drivers can be configured in an inverting or reverse configuration, where LED’s anode is connected to a negative v_O [28]. This is useful in systems that require negative supply rails. This -ve v_O is supplied and regulated by the SL power stage as illustrated in Fig. 2-6.

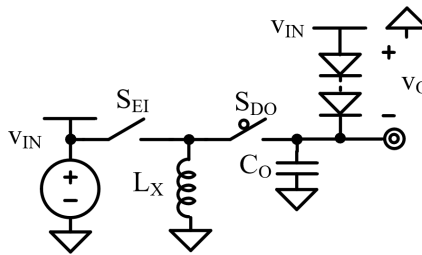


Figure 2-6. Inverting buck–boost SL driver.

Since de-energizing switches are disconnected from the LEDs during energizing phase, it is the output capacitance C_O that supplies LED current during that period. A larger C_O reduces Δi_{LED} . This necessitates its use in buck–boost and boost-based topologies, adding to the total solution space and cost [31].

2.2.3 Buck SL

As the name implies, buck SLs regulate v_{IN} to a lower v_O . Closing the input-connected switch S_{EI} drops a voltage of $v_{IN} - v_O$ across L_X which energizes directly into the output as shown in Fig. 2-7. S_{EI} then opens and ground connected switch S_{DG} closes with a $-v_O$ across L_X eventually

draining it. v_O is what current-regulated LEDs set (usually ~ 3 V/LED). The switch node voltage, therefore, swings between v_{IN} and ground during steady-state operation.

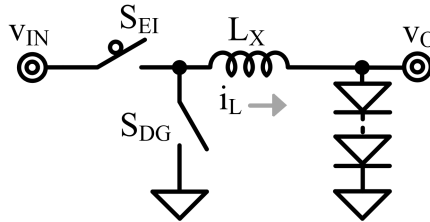


Figure 2-7. Buck SL driver.

Since bucks transfer while energizing, the inductor stores lesser energy than it transfers. As a result, i_L peaks to a lower value than in the buck–boost. Also, these require 2-lesser switches than buck–boost. These result in power savings in form of reduced ohmic, gate-charge, and I-V overlap losses. However, bucks can only output lower than v_{IN} limiting the number of series-connected LEDs.

2.2.4 Boost SL

As the name implies, boost SLs *boost* v_{IN} to a higher v_O which is set by the number of series-connected LEDs. Closing S_{EG} drops energizing voltage v_{IN} across L_X as Fig. 2-8 shows. On the other hand, a positive $v_O - v_{IN}$ de-energizes L_X as the output connected drain switch S_{DO} closes. This way, v_{IN} supplies power as L_X drains.

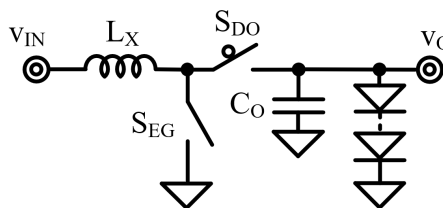


Figure 2-8. Boost SL driver.

Since boost SL transfers while draining, L_X stores lesser energy than it transfers. As a result, i_L peaks to a lower value than in the buck–boost. Boost has two fewer switches than the buck–boost, not surprisingly, boost is the part of buck–boost that boosts: L_X , S_{EG} , and S_{DO} . Like their buck counterparts, these reduce ohmic, I-V overlap, and gate drive power losses, therefore, leading to a higher η_C . However, boosts can only output higher than v_{IN} limiting the least number of series-connected LEDs [32].

2.3 Summary & Conclusions

This chapter presents a general DC–DC LED driver system and highlights encompassing switched inductor LED driver topologies popular in automotive applications, namely, linear, buck–boost, buck and boost. A brief discussion of their operation and corresponding advantages and disadvantages concludes SL to be better for high-power automotive applications where conversion efficiency is paramount.

With switched-inductor LED driver power stage, this research aims to analyze, access, and compare various aspects of LED dimming techniques. Therefore, this research generalizes the case of a buck–boost switched inductor power stage illustrated in Fig. 2-4 whose analysis can be easily carried over to other popular SL topologies [33]. Buck–boost is chosen for the ensuing analysis of dimming techniques in Chapters 3 and 4 given its wide range of applications and applicability of the theory and model to buck and boost SLs.

CHAPTER 3. ANALOG DIMMING

Figure 3-1 depicts a typical SL buck–boost LED driver power stage consisting of power switches (M_{EI} , M_{EG} , M_{DG} , M_{DO}), their corresponding gate drivers, and four series-connected power LEDs [31]–[32]. Switches M_{EI} and M_{EG} energize the inductor L_X from input v_{IN} during t_E , and M_{DG} and M_{DO} de-energize to output v_O during t_D . This occurs during the conduction period t_c , which is equal to switching period t_{sw} in Continuous Conduction Mode (CCM) as Fig. 3-2 shows. A drain duty-cycled fraction i_{DO} of inductor current i_L is delivered to the output, which the capacitor C_O filters to $i_{O(AVG)}$.

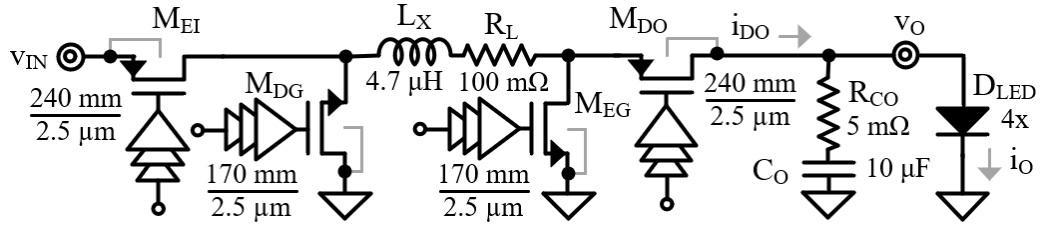


Figure 3-1. Switched inductor buck–boost LED driver power stage.

Energizing and drain duty cycles d_E and d_D are a t_E and t_D fraction of t_c . Furthermore, the relationship can be established as a function of v_{IN} and v_O [34], *i.e.*:

$$d_E \equiv \frac{t_E}{t_c} = 1 - d_D = 1 - \frac{v_{IN}}{v_{IN} + v_O}, \quad (3.1)$$

The average output LED current $i_{O(AVG)}$ is a d_D translation of the average inductor current, *i.e.*:

$$i_{O(AVG,CCM)} = i_{DO(AVG)} = i_{L(AVG)} d_D. \quad (3.2)$$

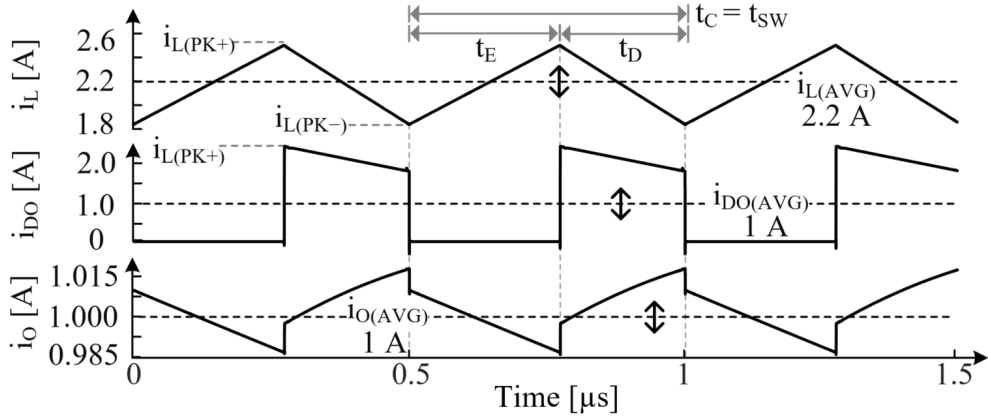


Figure 3-2. Simulated CCM operation.

SL transitions to Discontinuous Conduction Mode (DCM) as i_O decreases. L_X energizes during t_E , transfers energy during t_D and stops conducting as Fig. 3-3 shows. Varying t_{SW} with fixed i_L energy packets dims the average i_O . Like CCM, C_O filters the drain current ripple ($\Delta i_L = i_{L(PK+)}$) in DCM:

$$i_{O(AVG,DCM)} = i_{DO(AVG)} = i_{L(AVG)} d_D = \left(\frac{i_{L(PK)}}{2} \right) \left(\frac{t_C}{t_{SW}} \right) d_D. \quad (3.3)$$

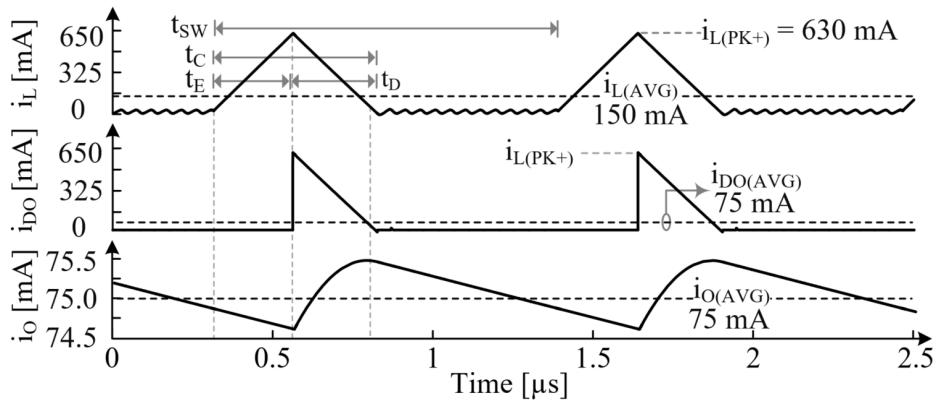


Figure 3-3. Simulated DCM operation.

3.1 Dimming Range

Sensing and controlling $i_{L(AVG)}$ and $i_{O(AVG)}$ over their entire range dims the LEDs as Figs. 3-2 and 3-3 shows. Since sparse i_L pulses can be delivered to the LEDs in DCM, the resulting $i_{O(AVG)}$ in (3.3) can be infinitesimally small. Therefore, analog dimming theoretically has a 0-100% dimming range.

3.2 Luminous Efficiency

Luminous efficiency η_L is light delivered per unit input power P_{IN} . Measured in lumens-per-watt, it is a cascaded measure of SL's η_C and LED's electro-optical efficiency η_{LED} :

$$\eta_L = \eta_C \eta_{LED} = \left(\frac{P_O}{P_{IN}} \right) \left(\frac{\phi_L}{P_O} \right), \quad (3.4)$$

where P_O is the fraction of power that SL delivers. As a result, quantifying η_L calls for modeling the luminous output ϕ_L and electrical parameters P_O , η_C , and P_{IN} . As Fig. 3-4 shows, ϕ_L (extracted from datasheet) varies exponentially with LED current i_O :

$$\phi_L \approx N_D \phi_k \left(1 - e^{-i_O/I_k} \right), \quad (3.5)$$

where N_D is the number of series-connected LEDs (*i.e.*, 4), and $\phi_k = 356$ and $I_k = 1.07$ are the modeled LED-dependent constants for cool-white CREE XP-E2 LED [17]. (3.5) can be rewritten as a logarithmic function of ϕ_L as:

$$i_O = \frac{1}{I_k} \ln \left(1 - \frac{\phi_L}{N_D \phi_k} \right)^{-1}. \quad (3.6)$$

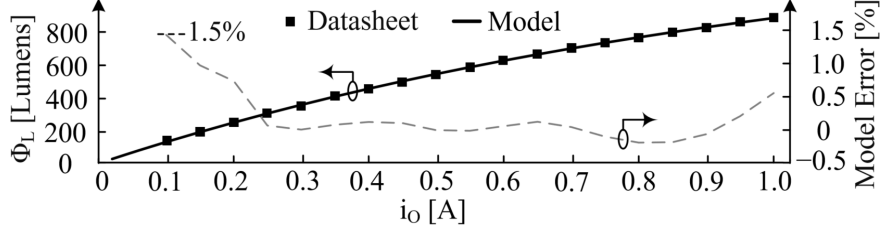


Figure 3-4. Luminous flux vs. output current for four CREE XP-E2 LEDs.

Since LEDs are electrically modeled as diodes [22], output voltage v_o as shown in Fig. 3-5 is a logarithmic and linear R_D translation of i_o :

$$v_o = N_D (v_D + v_R) = N_D \left(n_I v_T \ln \frac{i_o}{I_S} + i_o R_D \right), \quad (3.7)$$

where v_D is diode voltage, v_R is the voltage across LED parasitic resistance R_D , n_I is the diode non-ideality factor and I_S is the reverse saturation current.

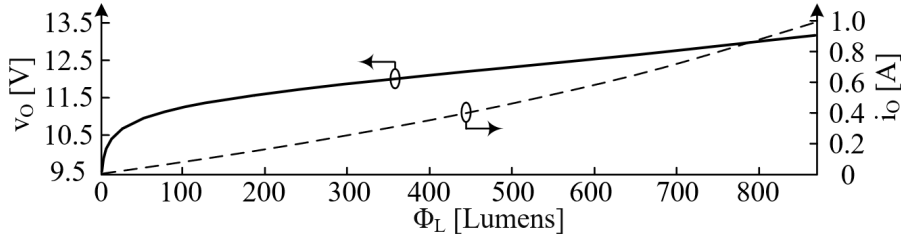


Figure 3-5. Output voltage and current vs. luminous flux.

Power conversion efficiency η_c for the buck–boost SL in Fig. 3-1 is shown in Fig. 3-6 [32]. When lightly loaded in DCM, the i_o that sets P_o is so low that controller (P_Q) and gate-charge (P_G) losses swamp all other losses. In this region η_c climbs because these losses do not scale with i_o . η_c peaks as power stage’s ohmic losses (P_R) match and surpass P_Q and P_G [34]. Power drawn P_{IN} is $1/\eta_c$ translation of P_o which is derived from (3.6), (3.7):

$$P_{IN} = \frac{P_O}{\eta_c} = \frac{v_O i_O}{\eta_c} \approx \frac{N_D (v_D + v_R)}{\eta_c} \left[-\frac{1}{I_k} \ln \left(1 - \frac{\phi_L}{\phi_k} \right) \right]. \quad (3.8)$$

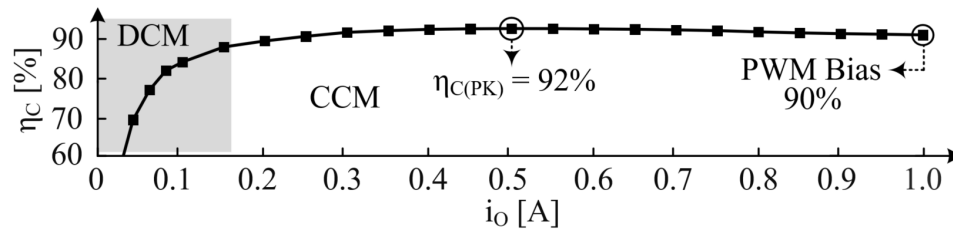


Figure 3-6. Simulated conversion efficiency vs. output current.

Simulated and modeled P_{IN} , which are within 1.5% of each other are depicted in Fig. 3-7. LED's ϕ_L climbs non-linearly with i_O as shown in Fig. 3-4. Therefore, a disproportionately higher P_O (and hence P_{IN}) are drawn to maintain a consistent increase in ϕ_L as Fig. 3-7 highlights.

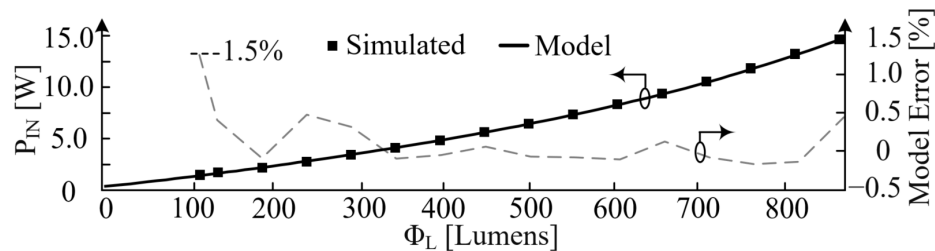


Figure 3-7. Modeled and simulated input power vs. luminous flux.

This non-linearity is also reflected in η_L as shown in Fig. 3-8. η_L falls at high ϕ_L s because disproportionately higher P_{IN} is needed to deliver same $\Delta\phi_L$. At low loads, SL power losses overwhelm P_O and eventually η_L peaks and drops.

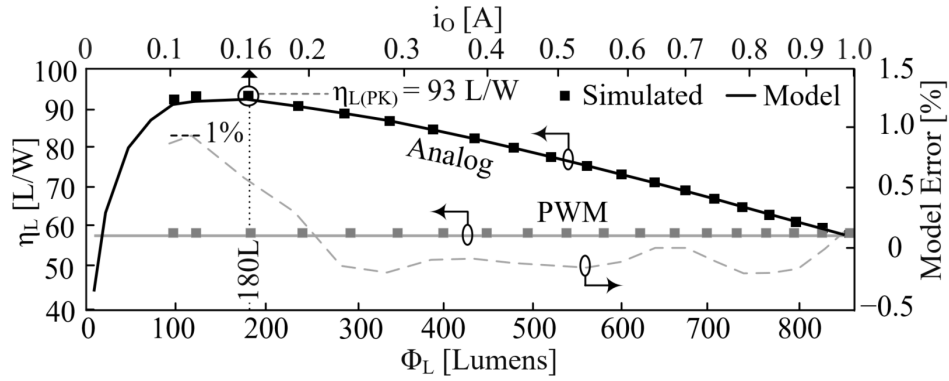


Figure 3-8. Modeled and simulated luminous efficiency vs. luminous flux.

3.3 Summary

This chapter analyzes the steady-state transient operation of a synchronous buck–boost and explains analog dimming in corresponding continuous and discontinuous conduction modes. Key parameters such as LED current, output voltage and input power are modeled using exponential-like expressions and verified against SPICE simulations. Finally, this analysis lays the framework for understanding and quantifying luminous efficiency. The following chapter expands over dimming techniques by detailing duty-cycled dimmers – their operation, dimming range analysis, advantages, and trade-offs in form of additional losses.

CHAPTER 4. DUTY-CYCLED DIMMING

Duty-cycled or pulse-width modulated (PWM) dimming is another way to dim the LEDs. Unlike analog, PWM achieves dimming by duty-cycling a fixed i_O at frequency much lower than SL's switching frequency f_{sw} . Typically, this duty-cycled frequency f_{PWM} is on the order of 0.1-1 kHz [1], [22] for automotive applications. Based on how it is achieved, it can be categorized as shutdown and its modified versions, shunt- and series-switched.

4.1 Shutdown

Operation: The simplest way to PWM-dim is by disabling the power-stage during PWM-OFF time $t_{PWM(OFF)}$ using an external dimming signal v_{DIM} [35]–[36]. This means opening M_{EI} and M_{EG} and draining the inductor via closed M_{DG} and M_{DO} . Exponentially decreasing i_O discharges C_O , turning the LEDs OFF as Fig. 4-1 shows. Note that primed variables are regulated non-dimmed currents and voltages.

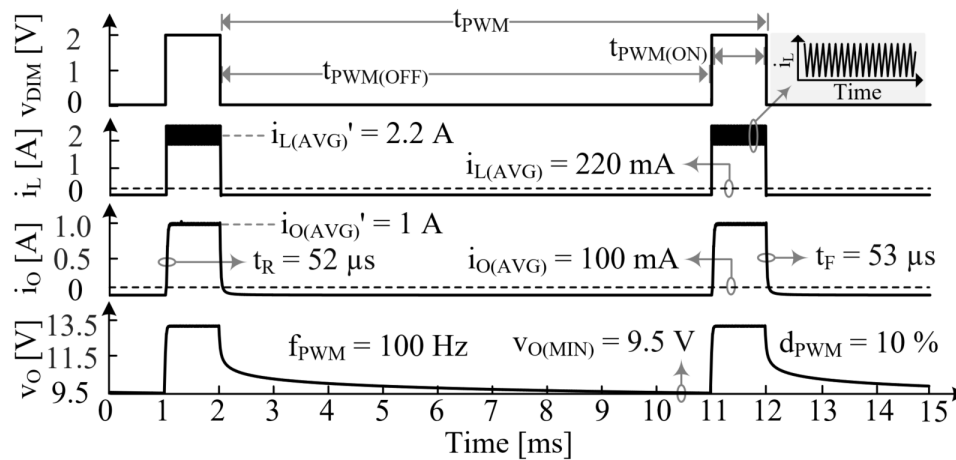


Figure 4-1. Shutdown duty-cycled dimming operation.

The average output current is a PWM duty cycle d_{PWM} fraction of duty-cycled average i_o' :

$$i_{O(\text{AVG})} = d_{\text{PWM}} i_{O(\text{AVG})}' = d_{\text{PWM}} d_D i_{L(\text{AVG})}', \quad (4.1)$$

where i_L' is the regulated inductor current. The power stage is then enabled with v_{DIM} , charges C_o linearly and operates normally during PWM-ON time $t_{\text{PWM(ON)}}$.

Dimming Range: Dimming range for PWM is like analog in a way that it is defined as minimum to maximum luminous output. ϕ_L is proportionate to $i_{O(\text{AVG})}$, which in PWM depends on minimum d_{PWM} :

$$d_{\text{PWM}} \geq \frac{t_R + t_F}{t_{\text{PWM}}}, \quad (4.2)$$

where t_R and t_F are the i_o rise and fall times respectively. t_{PWM} is the total period of the external PWM dimming signal v_{DIM} .

t_R and t_F consist of two components, inductor current slew t_L and output capacitor voltage slew t_C . When v_{DIM} turns on, SL switches and L_X slews to its regulation point i_L' , a reverse d_D translation of i_o' . Following this, SL transfers energy to the output and charges C_o . Similarly, at $t_{\text{PWM(OFF)}}$ instance L_X de-energizes to zero, followed by C_o discharge. Both t_R and t_F are represented by:

$$t_{R/F} = t_L + t_C = \left(\frac{L_X}{v_L} \right) \left(\frac{i_o'}{d_D} \right) + \frac{C_o \Delta v_o}{i_{C(\text{AVG})}}, \quad (4.3)$$

where v_L is the L_X voltage v_{IN} during energizing and v_o during the de-energizing phase and i_C is the charging or discharging C_o current. Δv_o is established from (3.7). Over t_R , average $i_{C(R)}$ is composed of the duty-cycled charging i_o' and discharging LED current i_o :

$$i_{C(R)(AVG)} = i_{O(AVG)}' - i_{O(R)(AVG)} \approx i_{L(AVG)}' d_D - \Delta i_{O(R)(AVG)}, \quad (4.4)$$

i_o is modeled as a straight line between 1-90% of average i_o' as shown in Fig. 4-2. During t_F , the $i_{C(F)}$ which is equivalent to i_o is exponentially modeled till i_o falls by 90%:

$$\begin{aligned} i_{C(F)(AVG)} &\approx i_{O(F)(AVG)} \\ &\approx \left(\frac{i_{O(AVG)}'}{2.3\tau} \right) \int_0^{2.3\tau} e^{-t/\tau} dt = i_{O(AVG)}' \left(\frac{1 - e^{-2.3}}{2.3} \right), \\ &= 39\% i_{O(AVG)}' \end{aligned} \quad (4.5)$$

where τ is the decaying time constant. Calculated t_R and t_F are over- and under-estimated as 58 μs and 43.6 μs which are within 18% of their simulated values. t_R 's and t_F 's inaccuracies systemically track and cancel each other. Consequently from (4.2) the minimum duty cycle is 1.05%, within 2% of simulations. Insightfully, larger C_O limits (dis-)charging rate and higher N_{DS} increase Δv_O thereby increasing $t_{R/F}$ proportionately.

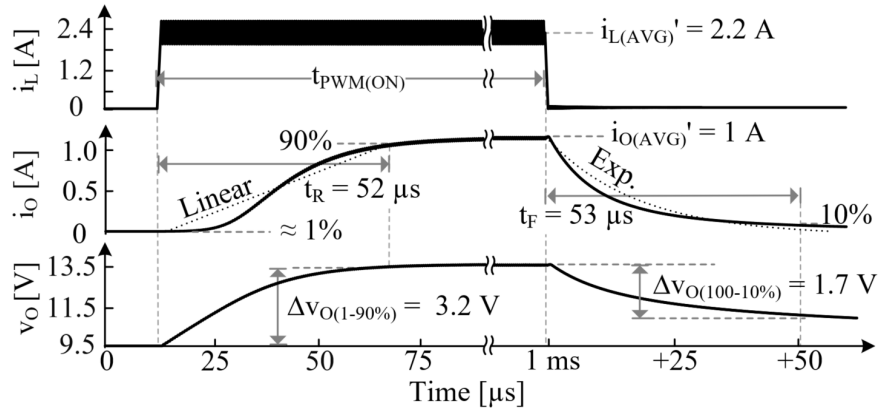


Figure 4-2. $t_{R/F}$ approximations for shutdown.

Power-Loss Analysis: Power stage conversion efficiency loss P_{SL} is common to both analog and duty-cycled dimming. Since ϕ_L tends to saturate at higher i_{OS} (from Fig. 3.4), duty-cycled dimming suffers from additional PWM power loss ΔP_{PWM} :

$$\Delta P_{P_{PWM}} = P_{IN(P_{PWM})} - P_{IN(A)} = P_{IN(A,PK)} d_{P_{PWM}} - P_{IN(A)}, \quad (4.6)$$

where $P_{IN(A,PK)}$ is the analog input power at peak $i_{O'}$ (*i.e.*, 1 A). $\Delta P_{P_{PWM}}$ is zero at both $i_{O'}$ extremes because analog and PWM dimming consume the same zero and peak P_{IN} as Fig. 4-2 shows.

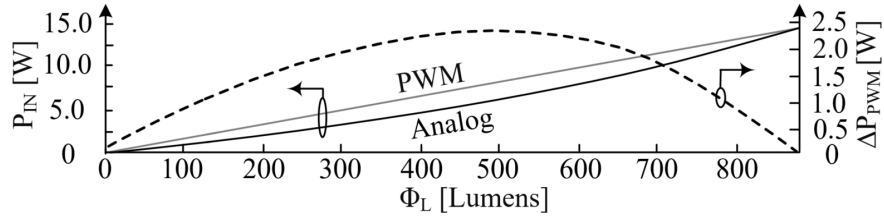


Figure 4-3. Input power and $P_{P_{PWM}}$ vs. luminous flux.

Because duty-cycled dimming has a fixed bias point at regulated $i_{O'}$, the corresponding η_C is 90% throughout the dimming range as Fig. 4-3 shows. All power losses are summarized in Fig. 4-4. Analysis reveals that $\Delta P_{P_{PWM}}$ dominates SL's power losses in both analog and PWM during majority of the dimming range, highlighting its inefficiency.

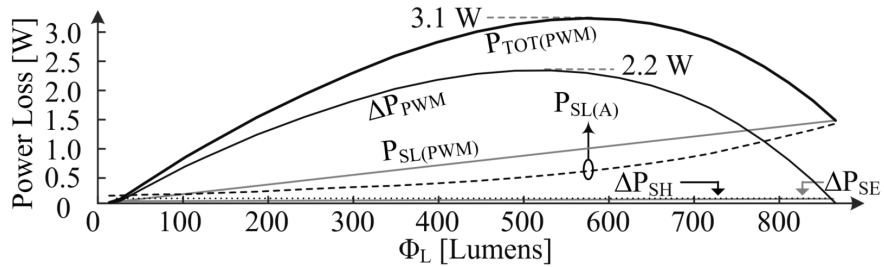


Figure 4-4. Breakdown of power losses in analog and PWM dimming.

4.2 Shunt-Switched

Shunt-switched PWM dimming technique modifies shutdown by incorporating switch $M_{P_{PWM}}$ in parallel to the LEDs as Fig. 4-5 shows. Closing $M_{P_{PWM}}$ along with disabling SL discharges C_O to ground, therefore turning off the LEDs. Similarly, at the PWM-ON instance $M_{P_{PWM}}$ opens and SL charges C_O which resumes normal LED operation as shown in Fig. 4-6.

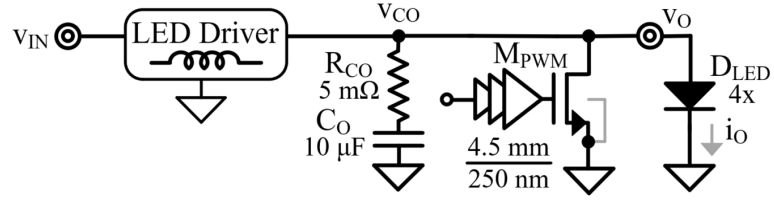


Figure 4-5. SL LED driver for shunt-switched dimming.

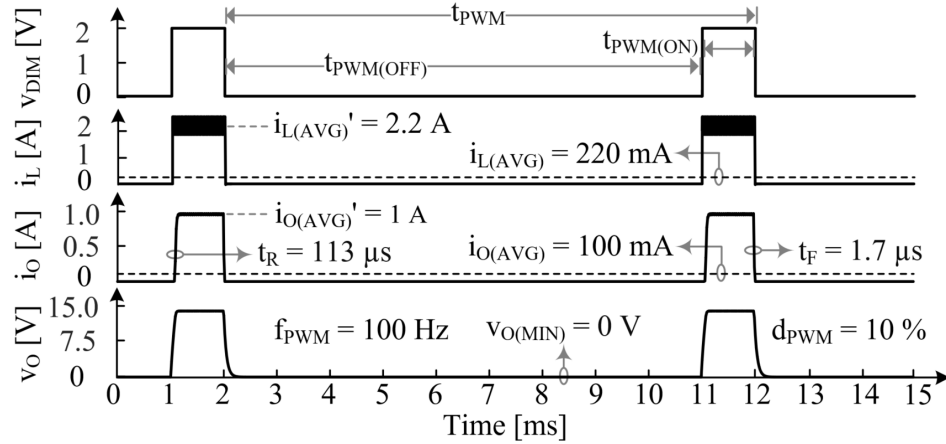


Figure 4-6. Shunt-switched PWM operation.

Additional Power Losses: Since M_{PWM} eventually shunts C_O to ground SL needs to recharge C_O to its regulated v_O' during $t_{PWM(ON)}$, which repeats every PWM cycle. Therefore, leading to a capacitor energy P_C loss of:

$$P_C \approx \frac{1}{2} C_O (v_{O(AVG)'})^2 f_{PWM} \quad (4.7)$$

SL delivers remnant L_X power P_L to C_O while turning-OFF, which is eventually shunted and dumped to ground:

$$P_L \approx \frac{1}{2} L_X (i_{L(AVG)'})^2 f_{PWM} \quad (4.8)$$

Furthermore, closing $M_{P_{PWM}}$ consumes gate-charge power P_G that v_{DD} supplies with charge q_G . q_G is the charge that overlap capacitance C_{OL} and channel capacitance C_{CH} , which constitute gate-drain and gate-source capacitances, need to close $M_{P_{PWM}}$:

$$P_G = v_{DD} \left(\frac{q_G}{t_{P_{PWM}}} \right) = v_{DD} q_G f_{P_{PWM}}, \quad (4.9)$$

$$q_G \approx C_{OL} (2v_{DD} + v_O) + C_{CH} \left(v_{DD} + \frac{v_{TN}}{4} \right). \quad (4.10)$$

These losses constitute the total additional power loss ΔP_{SH} in shunt-switched, which is miniscule as compared to the prominent P_{SL} and $\Delta P_{P_{PWM}}$ in Fig. 4-4. Fig. 4-7 depicts a breakdown of these additional losses. As shown, P_C overwhelms P_L and P_G and makes up the majority of ΔP_{SH} .

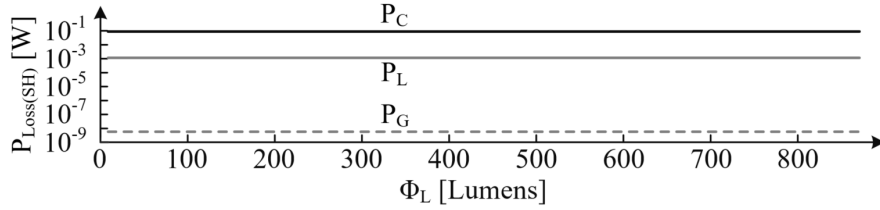


Figure 4-7. Breakdown of power losses in shunt-switched PWM dimming.

Dimming Range: Like shutdown, $t_{R/F}$ determines the minimum dimming range in shunt-switched PWM. Opening $M_{P_{PWM}}$ while switching SL pushes regulated i_L' to initially shunted C_O . LEDs conduct when C_O is sufficiently charged, *i.e.*, enough to allow 1% i_O' . t_R , therefore constitutes L_X 's i_L (t_L) and C_O 's v_O slew (t_C):

$$t_R = t_L + t_C \approx \frac{L_X}{v_L} \left(\frac{i_O'}{d_D} \right) + \frac{C_O \Delta v_{O(0-1\%)}}{i_{C(AVG)(0-1\%)}} + \frac{C_O \Delta v_{O(1-90\%)}}{i_{C(AVG)(1-90\%)}}. \quad (4.11)$$

v_O 's slew is divided into two components, when i_O rises from 0-1% i_O' and 1-90% i_O' as Fig. 4-8 shows. That is, one where drain duty-cycled i_L' flows just to C_O and when it is shared

with LEDs as i_{O} rises. The latter's $i_{C(AVG)}$ is approximated from (4.5). v_{O} 's steep increase during the former causes d_{D} to vary from 100% to 55% as per (3.1), which averaged over this duration is 73%. $i_{C(AVG)(0-1\%)}$ is therefore $d_{D(AVG)}i_{L(AVG)}$ '.

M_{PWM} closes in saturation because v_{O} (v_{DS}) is higher than a v_{TN} subtracted from v_{DD} (v_{GS}). Ten times i_{O} ' discharges C_{O} and hence steers current away from LEDs. M_{PWM} 's parameters W_{N} and L_{N} that support $10i_{O}$ ' can therefore be designed accordingly:

$$i_{C(F)} \approx i_{PWM(SAT)} \equiv 10i_{O(AVG)'} = \frac{1}{2}K_{N}'\left(\frac{W_{N}}{L_{N}}\right)(v_{DD} - v_{TN})^2. \quad (4.12)$$

Consequently, t_{F} is the time in which $10i_{O}$ ' discharges C_{O} by $\Delta v_{O(F)}$ to when i_{O} falls by 90%:

$$t_{F} \approx \frac{C_{O}\Delta v_{O(100-10\%)}}{i_{C(F)}}. \quad (4.13)$$

Calculated t_{R} and t_{F} are 118 μs and 1.65 μs which are within 8% and 3% of simulations. This puts dimming range of 1.15% within 4% of its simulations.

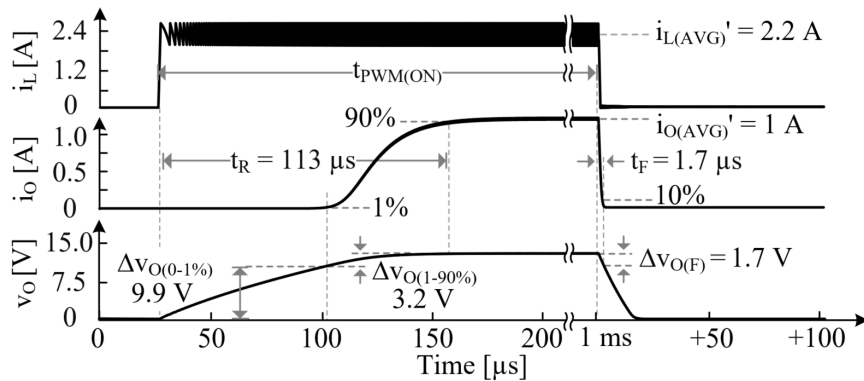


Figure 4-8. $t_{R/F}$ for shunt-switched PWM.

4.3 Series-Switched

Series-switched PWM dimming is another modification to SL shutdown [37]. In addition to the power stage shutdown, series-connected PMOS M_{PWM} switches i_O with v_{DIM} as shown in Figs. 4-9 and 4-10.

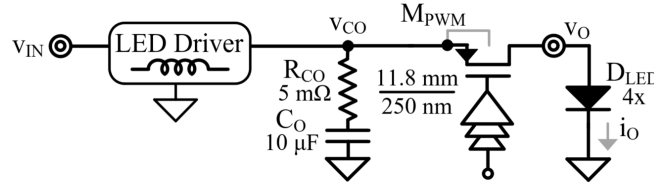


Figure 4-9. SL LED driver for series-switched dimming.

At PWM-ON instance, SL switches to energize L_X to its i_L' . Followed by an energizing L_X slew delay t_{PRE} , M_{PWM} connects SL to the LED load:

$$t_{PRE} \approx \left(\frac{L_X}{v_{IN}} \right) i_{L(AVG)'} \quad (4.14)$$

This SL pre-charge mechanism [38] in-tandem with C_O 's v_{CO} preservation (discussed later) during $t_{PWM(OFF)}$ allows instantaneous LED current rise. Like shunt-switched, SL is disabled when M_{PWM} disconnects, which limits C_O overcharge.

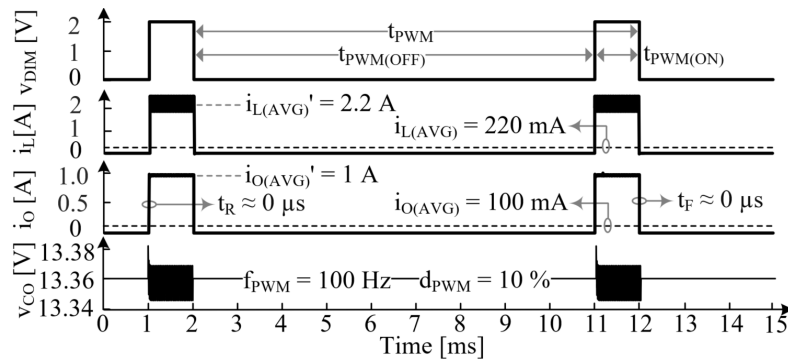


Figure 4-10. Series-switched PWM operation.

Additional Power Losses: SL delivers remnant L_X power P_L to C_O while turning-OFF which can lead to an overcurrent spike at the $t_{P_{WM}(ON)}$ instance, stressing the LEDs and other output-connected circuitry. A solution is to maintain output capacitor voltage v_{CO} during $t_{P_{WM}(OFF)}$. Variations of this concept have been implemented in modern LED drivers [37]–[43]. Maintaining v_O implies excess P_L in (4.8) is disregarded. Additionally, $M_{P_{WM}}$'s ohmic loss $P_{R(SW)}$ contributes to the overall ΔP_{SE} loss, *i.e.*,

$$P_{R(SW)} = (i_{O(AVG)})^2 R_{P_{WM}} d_{P_{WM}}, \quad (4.15)$$

$$R_{P_{WM}} \equiv R_{CH} = \frac{1}{K_P \left(\frac{W_P}{L_P} \right) (v_{DD} - |v_{TP}|)}. \quad (4.16)$$

For a typical 100 m Ω resistance $P_{R(SW)}$ is 100 mW at peak i_O ' of 1 A. An inductor power loss P_L of 1.1 mW and gate charge loss P_G of 14.9 nW are further lost as per (4.9) and (4.10) as Fig. 4-11 shows.

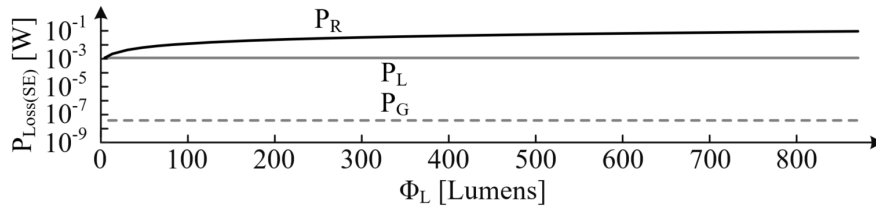


Figure 4-11. Breakdown of power losses in series-switched PWM dimming.

Dimming Range: $M_{P_{WM}}$ instantaneously connects SL power stage to the LEDs as soon as L_X slews to its regulation point. Larger C_O reduces Δv_{CO} because of L_X energy transfer during this connection instance. Therefore limiting Δi_O such that peak i_O is always within 10% i_O' as Fig. 4-12 shows. Eventually, switching dynamics of $M_{P_{WM}}$ determine the t_R and t_F , which can be as low as a few nanoseconds providing a dimming capability of up to 0% for a 100 Hz dimming signal.

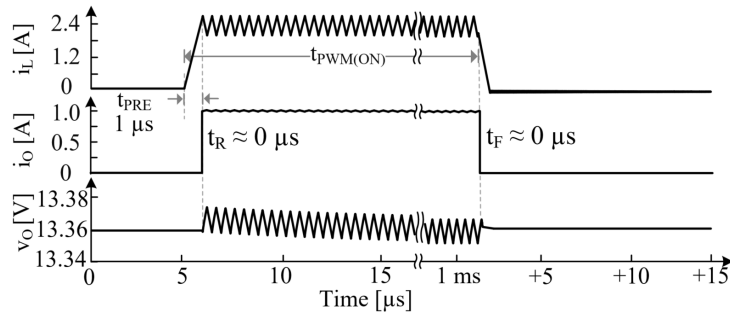


Figure 4-12. $t_{R/F}$ for series-switched PWM.

4.4 Luminous Efficiency

Since luminous output and drawn P_{IN} are the same duty-cycled fraction of the peak biasing point i_o' , η_L is constant across the dimming range as Fig. 3-8 illustrates. Furthermore, PWM dimming draws more power for the same amount of light as Fig. 4-3 shows reducing its luminous efficiency. Revealing that analog dimming is up to 57% more efficient over PWM.

4.5 Summary

This chapter presents duty-cycled (PWM) LED dimming techniques. It begins with the simplest, *shutdown* technique, which achieves dimming by duty-cycling a fixed LED current (for example, 1 A). As the name suggests, this is accomplished by disabling the LED driver. Circuit analysis explains and avails key parameters such as dimming range which depends on i_{LED} 's rise and fall time which in turn depend on C_O and N_{LED} . This chapter also reveals a fundamental luminous (and power) loss associated with PWM dimming. Basic shutdown is further modified by adding an output-connected shunt- or series-switch. Aptly named, the shunt-switched technique dims by shunting the LEDs to 0 V. Whereas series-switched, in addition to shutdown, instantaneously disconnects them from SL. Both techniques lead to additional albeit negligible power losses and need more space because of an extra MOS switch.

CHAPTER 5. CONCLUSIONS AND FUTURE WORK

5.1 Conclusions

Table 5-1 provides an overview and compares analog and duty-cycled dimming techniques. Analog dimming yields the highest η_L , up to 57% more, over most of the luminous range as Fig. 3-8 shows. However, at low loads when SL losses outpace power delivered, $\eta_{L(PWM)}$ overtakes. Hybrid dimming approaches where LED driver can modulate i_O during PWM have been proposed to improve PWM η_L but it complicates control and requires additional current channels [1], [26], [44]. Therefore, reducing its popularity.

Although analog dimming technique theoretically promises up to 0% dimming, in practice it is a function of i_O or i_L sensing accuracy, noise and offsets, which can be improved by design [31], [35]. Furthermore, it also depends on LED's luminous characteristics. That is, if they can emit light at low enough i_O .

The effects of dimming techniques on the color spectrum in high-power commercial white LEDs are widely studied in state-of-the-art [45] – [48]. Variations in the spectrum are a function of i_{LED} and junction temperature T_J . However, the chromaticity co-ordinates [45] shift less than 1% with i_{LED} [46] for both analog and duty-cycled, which is considered negligible [48] for automotive applications. Moreover, automotive systems employ heat sinks to operate at fixed junction temperature which further minimizes the spectral shifts.

Shutdown dimming technique is often used in buck SLs where large C_O s are not needed to supply i_O during t_E [50] – [52]. Therefore, reducing its $t_{R/F}$ and improving the dimming range. In boost SLs, L_X 's DC-short and body-diode conduction of M_{DO} eventually forces v_O to v_{IN}

when shutdown. However, since typical boost SL's v_O is 2-4x when operational [37], [39] and because of LEDs exponential I-V relationship i_O is negligible.

Shunt- and series-switched PWM dimming can also be extended to buck and boost SL topologies as Figs. 5-1(a)-(d) show. Dimming in boost using series-switched as depicted in Fig. 5-1(a) operates in the exact same way as buck–boost. However, grounding $S_{P\text{WM}}$ during shunt-switched PWM would undesirably energize L_X via body-diode D_{DO} as Fig. 5-1(b) depicts. Directly shunting to v_{IN} instead of ground counters this.

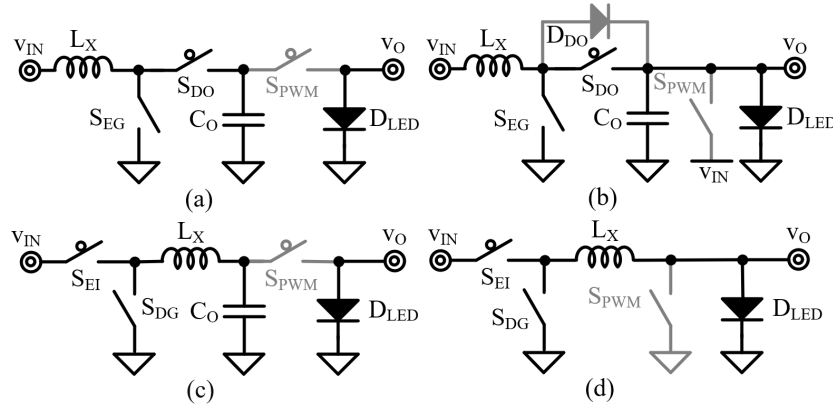


Figure 5-1. Buck and boost implementations of series- and shunt-switched PWM.

Buck topologies operate like their boost-based counterparts when series-switched as shown in Fig. 5-1(c). C_O absorbs additional P_L when S_{PWM} reconnects, limiting Δv_{CO} and Δi_O . Contrary to buck–boost, bucks need not shutdown when shunt-switched [25], [53]. This is because they can de-energize to the ground when S_{PWM} closes in Fig. 5-1(d). Not shutting SL also improves their dimming capabilities since L_X need not slew when SL restarts. However, this costs additional S_{PWM} 's ohmic and SL's switching and ohmic power during $t_{\text{PWM(OFF)}}$.

TABLE 5-1. Comparing analog and duty-cycled dimming.

Parameter	Analog	Duty-cycled (PWM)		
		Shutdown	Shunt-SW	Series-SW
η_L	45-93 L/W	59 L/W		
Space	—	Same as Analog	Additional M_{PWM}	
i_o 's $t_R + t_F$	N/A	$\leq 100 \mu s$	$\leq 120 \mu s$	$\leq 10 ns$
Dim. Range	0-100%	1-100%	1.2-100%	≈ 0 -100%
SL η_C Loss	0.18-1.4 W	$\leq 1.4 W$		
ΔPWM Loss	No loss	$\leq 2.2 W$		
Add. Losses	N/A		$P_C + P_L + P_G$	$P_R + P_L + P_G$
References	[31]–[32]	[36], [54]	[25], [53]	[37]–[43], [55]

$V_{IN} = 12 V$, $N_D = 4$, $v_O \approx 13.3 V$, $f_{SW(CCM)} = 2 MHz$, $v_{DD} = 2 V$, $L_X = 4.7 \mu H$, $C_O = 10 \mu F$, $f_{PWM} = 100 Hz$, $K_{N'} = 200 \mu A/V^2$, $K_{P'} = 100 \mu A/V^2$, $|v_{TN/P}| = 0.4 V$

Published contribution: This research has been published in the following peer-reviewed conference:

[1] V. Gupta and G.A. Rincon-Mora, "Dimming DC-DC LED Drivers: Luminous Efficiency, Power Losses, & Best-in-Class," in *IEEE Ind. Electronics Conf. (IECON)*, Toronto, Canada, 2021.

5.2 Future Directions

Hybrid dimming approaches where LED drivers can modulate LED current during PWM have been proposed in the state of the art to improve PWM η_L [1], [26], [44]. However, rigorous analysis in practical integrated designs is needed to evaluate their advantages and drawbacks. Furthermore, simulations and experimental results are crucial to brainstorm and quantify the parameters for such methods. As a result, the next step in this research would be to conduct those using the analysis techniques presented in this research.

REFERENCES

- [1] K. H. Loo, W. Lun, S. Tan, Y. M. Lai, and C. K. Tse, "On driving techniques for LEDs: Toward a generalized methodology," *IEEE Transactions on Power Electronics*, vol. 24, no. 12, pp. 2967-2976, Dec. 2009.
- [2] A. N. Krasnov, "Electroluminescent displays: history and lessons learned," *Displays*, vol. 24, no. 2, pp. 73-79, Aug. 2003.
- [3] W. Chen, S. Y. R. Hui, "Elimination of an electrolytic capacitor in AC/DC light-emitting diode (LED) driver with high input power factor and constant output current," *IEEE Transactions on Power Electronics*, vol. 27, no. 3, pp. 1598-1607, Mar. 2012.
- [4] M. Arias, A. Vazquez, and J. Sebastian, "An overview of the AC-DC and DC-DC converters for LED lighting applications," *Automatika Journal for Control, Measurement, Electronics, Computing and Communications*, vol. 53, no. 2, pp. 156-172, May 2012.
- [5] H. Kim, B. Lee, and C.-T. Rim, "Passive LED driver compatible with rapid-start ballast," in *International Conference on Power Electronics (ECCE Asia)*, 2011, pp. 507-514.
- [6] M. R. Krames, O. B. Shchekin, R. Mueller-Mach, G. O. Mueller, L. Zhou, G. Harbers, and M. G. Craford, "Status and future of high-power light-emitting diodes for solid-state lighting," *Journal of Display Technology*, vol. 3, no. 2, pp. 160-175, 2007.
- [7] A. Vemuri, "Trends and topologies for automotive rear lighting systems," Oct. 2019. Available: www.ti.com/lit/wp/szzy011a/szzy011a.pdf
- [8] S. Li, S. Tan, C. K. Lee, E. Waffenschmidt, S. Y. R. Hui, and C. K. Tse, "A survey, classification, and critical review of light-emitting diode drivers," *IEEE Transactions on Power Electronics*, vol. 31, no. 2, pp. 1503-1516, Feb. 2016.
- [9] Y. Wang, J. M. Alonso, and X. Ruan, "A review of LED drivers and related technologies," *IEEE Transactions on Industrial Electronics*, vol. 64, no. 7, pp. 5754-5765, July 2017.
- [10] M. Khatua, *et al.*, "High-performance megahertz-frequency resonant DC-DC converter for automotive LED driver applications," *IEEE Transactions on Power Electronics*, vol. 35, no. 10, pp. 10396-10412, Oct. 2020.
- [11] L. Cheng, *et al.*, "On-chip compensated wide output range boost converter with fixed-frequency adaptive off-time control for LED driver applications," *IEEE Transactions on Power Electronics*, vol. 30, no. 4, pp. 2096-2107, Apr. 2015.

- [12] B. Wu, Z. Ye, "Comprehensive power supply system designs for harsh automotive environments consume minimal space, preserve battery charge, feature low EMI," *Analog Dialogue*, vol. 53, no. 3, pp. 40-48.
- [13] C. Wallace, "LED driver basics," 2018. Available: <https://training.ti.com/led-driver-basics>.
- [14] Osram Opto Semiconductors GmbH, "OSLON Black Flat," Model KW H2L531.TE, www.osram.com/os/products/product-promotions/led-for-automotive-industry-and-consumer-applications/oslon_black_flat_family.jsp.
- [15] SMART Global Holdings Inc., Model XLamp XP-G2, cree-led.com/products/xlamp-leds-discrete/xlamp-xp-g2.
- [16] Lumileds Holding B.V., Model LUXEON F ES Cool White, lumileds.com/products/single-die-leds/luxeon-f/.
- [17] SMART Global Holdings Inc., Model XLamp XP-E2, cree-led.com/products/xlamp-leds-discrete/xlamp-xp-e2.
- [18] SMART Global Holdings Inc., Model XLamp XQ-E, cree-led.com/products/xlamp-leds-discrete/xlamp-xq-e.
- [19] Osram Opto Semiconductors GmbH, "OSLON LX ECE," Model LUW CVBP.CE, www.osram.com/ecat/OSLON@%20LX%20ECE%20LUW%20CVBP.CE/com/en/class_pim_web_catalog_103489/prd_pim_device_2190858/.
- [20] Lumileds Holding B.V., Model LUXEON Altilon Intense, lumileds.com/products/multi-die-leds/luxeon-altilon-intense/.
- [21] SMART Global Holdings Inc., Model XLamp XQ-A, cree-led.com/products/xlamp-leds-discrete/xlamp-xq-e.
- [22] Z. Dong, C. K. Tse, and S. Y. R. Hui, "Circuit theoretic considerations of LED driving: Voltage-source versus current-source driving," *IEEE Transactions on Power Electronics*, vol. 34, no. 5, pp. 4689-4702, May 2019.
- [23] Y. Hu and M. M. Jovanovic, "LED driver with self-adaptive drive voltage," *IEEE Transactions on Power Electronics*, vol. 23, no. 6, pp. 3116-3125, Nov. 2008.
- [24] E. Cheung, "High voltage boost/LED controller provides 3000:1 PWM dimming ratio," *Analog Devices*, Mar. 2006.
- [25] R. Rosen, "Dimming techniques for switched-mode LED drivers," 2009. Available: www.ti.com/lit/an/snva605/snva605.pdf.
- [26] S. Tan, "General n-level driving approach for improving electrical-to-optical energy-conversion efficiency of fast-response saturable lighting devices," *IEEE Transactions on Industrial Electronics*, vol. 57, no. 4, pp. 1342-1353, Apr. 2010.

- [27] G. A. Rincón-Mora, "*Switched-Inductor Power Supplies*," 2019.
- [28] Analog Devices Inc., "High current synchronous step-down LED driver," Model LT3744, www.analog.com/en/products/lt3744.html.
- [29] J. Garcia, A. J. Calleja, E. L. Corominas, D. G. Vaquero and L. Campa, "Interleaved buck converter for fast PWM dimming of high-brightness LEDs," *IEEE Transactions on Power Electronics*, vol. 26, no. 9, pp. 2627-2636, Sept. 2011.
- [30] D. Park, Z. Liu and H. Lee, "A 40 V 10 W 93%-efficiency current-accuracy-enhanced dimmable LED driver with adaptive timing difference compensation for solid-state lighting applications," *IEEE Journal of Solid-State Circuits*, vol. 49, no. 8, pp. 1848-1860, Aug. 2014.
- [31] S. Rao, Q. Khan, S. Bang, D. Swank, A. Rao, W. McIntyre, and P. K. Hanumolu, "A 1.2-A buck-boost LED driver with on-chip error averaged senseFET-based current sensing technique," *IEEE Journal of Solid-State Circuits*, vol. 46, no. 12, pp. 2772-2783, Dec. 2011.
- [32] Analog Devices Inc., "36V, 2A synchronous buck-boost converter and LED driver," Model LT3942, www.analog.com/en/products/lt3942.html.
- [33] Y. Qin, S. Li and S. Y. Hui, "Topology-transition control for wide-input-voltage-range efficiency improvement and fast current regulation in automotive LED applications," *IEEE Transactions on Industrial Electronics*, vol. 64, no. 7, pp. 5883-5893, July 2017.
- [34] G. A. Rincón-Mora, "*Power IC design: top-down approach*," Lulu Press Inc., Morrisville, North Carolina, 2016.
- [35] P. Malcovati, M. Belloni, F. Gozzini, C. Bazzani, and A. Baschiroto, "A 0.18- μ m CMOS, 91%-efficiency, 2-A scalable buck-boost DC-DC converter for LED drivers," *IEEE Transactions on Power Electronics*, vol. 29, no. 10, pp. 5392-5398, Oct. 2014.
- [36] Q. Cheng and H. Lee, "A high-frequency non-isolated ZVS synchronous buck-boost LED driver with fully-integrated dynamic dead-time controlled gate drive," in *IEEE Applied Power Electronics Conference and Exposition (APEC)*, Mar. 2018, pp. 419-422.
- [37] X. Xiaoru and W. Xiaobo, "High dimming ratio LED driver with fast transient boost converter," in *IEEE Power Electronics Specialists Conference (PESC)*, Jun. 2008, pp. 4192-4195.
- [38] K. S. Yoon and K. Lee, "A CMOS high dimming ratio power-LED driver with a preloading inductor current method," in *International Symposium on Quality Electronic Design (ISQED)*, Mar. 2013, pp. 709-713.
- [39] M. Zhou, L. Cheng, D. Lv, Z. Hong, and B. Y. Liu, "A dual-path, current-sensing resistor-free boost LED driver with fast PWM dimming," in *IEEE Applied Power Electronics Conference and Exposition (APEC)*, Mar. 2013, pp. 848-853.

- [40] Y. Hsieh, *et. al.*, "A high-dimming-ratio LED driver for LCD backlights," *IEEE Transactions on Power Electronics*, vol. 27, no. 11, pp. 4562-4570, Nov. 2012.
- [41] P. R. Surkanti and P. M. Furth, "High-efficiency, high-dimming ratio LED driver," in *IEEE International Midwest Symposium on Circuits and Systems (MWSCAS)*, Aug. 2013, pp. 360-363.
- [42] S. Li, Y. Guo, A. T. L. Lee, T. Siew Chong, and S. Y. R. Hui, "Precise and full-range dimming control for an offline single-inductor-multiple-output LED driver," in *IEEE Energy Conversion Congress and Exposition (ECCE)*, Sept. 2016, pp. 1-7.
- [43] J. Caldwell, D. Kwon, L. Milner, "Maintaining output capacitance voltage in led driver systems during PWM off times," United States Patent 9596728, Mar. 14, 2017.
- [44] Y. Zhang, G. Rong, S. Qu, Q. Song, X. Tang, and Y. Zhang, "A high-power LED driver based on single inductor-multiple output DC–DC converter with high dimming frequency and wide dimming range," *IEEE Transactions on Power Electronics*, vol. 35, no. 8, pp. 8501-8511, Aug. 2020.
- [45] K. H. Loo, Y. M. Lai, S. Tan, and C. K. Tse, "Stationary and Adaptive Color-Shift Reduction Methods Based on the Bilevel Driving Technique for Phosphor-Converted White LEDs," *IEEE Transactions on Power Electronics*, vol. 26, no. 7, pp. 1943-1953, 2011.
- [46] K. H. Loo, Y. M. Lai, S. Tan, and C. K. Tse, "On the color stability of phosphor-converted white LEDs under DC, PWM, and bilevel drive," *IEEE Transactions on Power Electronics*, vol. 27, no. 2, pp. 974-984, Feb. 2012.
- [47] O. V. Khokhlev, M. S. Ramm, and S. Y. Karpov. "Effect of temperature and current variations on the color quality of white light emitting diodes." Available: http://load.strsoft.com/Data11/SimuLED/Publications/LS12_WhiteLED3_Poster.pdf
- [48] S. Keeping, "LED color shift under PWM dimming," 2014. Available: <https://www.digikey.com/en/articles/led-color-shift-under-pwm-dimming>
- [49] Q. Cheng, J. Liu, and H. Lee, "A 5-100V input low-profile adaptive delay compensated hysteretic LED driver with enhanced current accuracy," in *IEEE Custom Integrated Circuits Conference (CICC)*, Apr. 2021.
- [50] Y. Qu, W. Shu, and J. S. Chang, "A low-EMI, high-reliability PWM-based dual-phase LED driver for automotive lighting," *IEEE Journal of Emerging and Selected Topics in Power Electronics*, vol. 6, no. 3, pp. 1179-1189, Sep. 2018.
- [51] Y. Qu, W. Shu, and J. S. Chang, "A 2.8-MHz 96.1%-peak-efficiency 1.4- μ s-settling-time fully soft-switched LED driver with 0.08–1 dimming range," *IEEE Transactions on Power Electronics*, vol. 34, no. 10, pp. 10094-10104, Jan. 2019.

- [52] Z. Liu and H. Lee, "A 26 W 97%-efficiency fast-settling dimmable LED driver with dual-nMOS-sensing based glitch-tolerant synchronous current control for high-brightness solid-state lighting applications," *IEEE Journal of Solid-State Circuits*, vol. 50, no. 9, pp. 2174-2187, May 2015.
- [53] Y. Wang, X. Wu, Y. Hou, P. Cheng, Y. Liang, and L. Li, "Full-range LED dimming driver with ultrahigh frequency PWM shunt dimming control," *IEEE Access*, vol. 8, pp. 79695-79707, Aug. 2020.
- [54] L. Corradini and G. Spiazzi, "A high-frequency digitally controlled LED driver for automotive applications with fast dimming capabilities," *IEEE Transactions on Power Electronics*, vol. 29, no. 12, pp. 6648-6659, Dec. 2014.
- [55] Analog Devices Inc., "36V, 2.3A synchronous step-up LED driver with 25,000:1 PWM dimming," Model LT3922-1, <https://www.analog.com/en/products/lt3922-1.html>.